Energy structure and far-infrared spectroscopy of two electrons in a self-assembled quantum ring

2005 J. Phys.: Condens. Matter 17 1573

(http://iopscience.iop.org/0953-8984/17/10/012)

INSTITUTE OF PHYSICS PUBLISHING JOURNAL OF PHYSICS: CONDENSED MATTER

J. Phys.: Condens. Matter **17** (2005) 1573–1582 doi:10.1088/0953-8984/17/10/012

Energy structure and far-infrared spectroscopy of two electrons in a self-assembled quantum ring

J I Climente, J Planelles and F Rajadell

Departament de Ciències Experimentals, UJI, Box 224, E-12080 Castelló, Spain

E-mail: planelle@exp.uji.es

Received 29 September 2004, in final form 1 February 2005
Published 25 February 2005
Online at stacks.iop.org/JPhysCM/17/1573

Abstract

The energy levels and far-infrared absorption spectra of a self-assembled InAs ring with one and two electrons in an external magnetic field are calculated numerically. We use a truly three-dimensional effective mass model which considers finite potential barriers and mass dependence on the energy and position, and includes strain effects. The results obtained indicate that far-infrared spectroscopy of self-assembled rings is very sensitive to electron–electron interactions. The exchange energy leads to aperiodic fractional Aharonov–Bohm oscillations of electronic states and rapid narrowing of the magnetic field windows corresponding to the spin singlet ground state. Our results also suggest that the symmetric form of parabolic confinement potential, which has been widely employed to describe quantum rings, is unsuitable for self-assembled rings as it poorly describes the relevant effects of the inner radius.

1. Introduction

Recent advances in nanoscopic fabrication techniques have made it possible to grow self-organized InAs nanorings with 'volcano' shapes [1, 2]. These nanoscopic rings may be the best suited quantum structures for investigating the electronic and optical properties of quantum rings, because they are in the scattering-free and few-particle limit [5]. Two of the most interesting properties of quantum rings are their response to external magnetic fields and their multi-particle excitation spectra. In the presence of a magnetic field, perpendicular to the plane of the ring, the interaction between the charge of a particle confined in the ring and the magnetic flux induces successive changes of the carrier ground state symmetry (i.e. the Aharonov–Bohm (AB) effect [3]). In addition, the ringlike confinement breaks down the generalized Kohn theorem so that, unlike in quantum dots, the excitation spectrum of quantum rings may reveal electron–electron interaction effects [4].

In order to study these properties Lorke and co-workers measured the far-infrared (FIR) magneto-absorption spectra of a macroscopic number of self-assembled quantum rings, each of them charged on average with two electrons [5]. Despite of the fact that several theoretical works have studied electron–electron interactions in these structures [5–9], the role of such interactions is not very clear yet. For example, some authors suggested that the profile of Lorke's FIR spectroscopy experiment is roughly captured by the non-interacting particles picture [5, 7]. This is surprising because the Coulomb energy inferred from capacitance experiments for a two-electron self-assembled ring was as large as 20 meV [5], and therefore the so-called 'fractional AB effect' should yield major changes in the energy structure [10, 11]. Other authors obtained a similar degree of agreement with the FIR experiment by considering interacting particles [6]. The energy spectrum they predicted for the non-interacting case was indeed different to that they predicted for the interacting case.

The fact that both the non-interacting and interacting pictures account for most of the experimental data can be explained from two factors. On the one hand, the theoretical models used so far to investigate Lorke's two-electron experiment were based on the two-dimensional effective mass Hamiltonian with parabolic confinement potential introduced by Chakraborty *et al* [12]. Such models are subject to a fitting procedure[1] which warrants agreement with a number of experimental resonances. On the other hand, the low resolution of the FIR absorption experiment allowed only the detection of a small number of resonances. No resonance under 10 meV could be registered. Therefore, a significant part of the experimental data may be reproduced by means of either the non-interacting or the interacting Hamiltonian with an appropriate fitting procedure. A theoretical model free of fitting parameters is of high interest in order to unambiguously determine the role of electron–electron interactions in self-assembled quantum rings.

Moreover, there are doubts regarding the validity of the parabolic confinement potential for self-assembled quantum rings. The electronic states of these rings are very sensitive to changes in the inner radius [14]. Thus, unlike in quantum dots, the details of the confinement potential are important. Using a confinement potential of the form introduced in [12] and assuming that a single ring geometry was present in the sample of [5], reasonable agreement with the experimental FIR resonances was obtained [5–7]. Conversely, a later work by Puente and Serra [8] using a different form of parabolic confinement potential (which was modified to account better for the inner radius of the ring) required a bimodal distribution of ring sizes to explain the same experimental data. It follows that a realistic confinement potential is needed for a definitive assessment of the role of the electron–electron repulsion on the optoelectronic properties of a self-assembled ring with interacting electrons.

In this paper, we use a truly three-dimensional model, similar to those which successfully described the near-infrared spectrum [15] and single-electron energy structure [16, 17] of InGaAs rings, to calculate the electron states and intraband transitions of one and two electrons in a typical InAs/GaAs quantum ring. We use a finite rectangular-well confinement potential defined by the band offset between the material of the ring and that of the matrix. Without any additional knowledge on the possible interface grading or bandbending, this potential is certainly the most reasonable that one can propose[2].

[1] At least three parameters need to be fitted: the *characteristic frequency* of the confinement potential, the *effective radius* of the ring and the electron two-dimensional effective mass [12, 13].

[2] It should be noted that the asymmetry of the 2D parabolic-like potential of [8] accounts for the unequal vertical confinement at the inner and outer edges of the ring cross-section: an abrupt potential for the inner edge, which represents the sheer wall of the ring cavity, and a smoothly increasing potential for the outer edge, which represents the smoothly decreasing height of the ring in the radial direction. Since our confinement potential is 3D, it accounts for this vertical confinement explicitly.

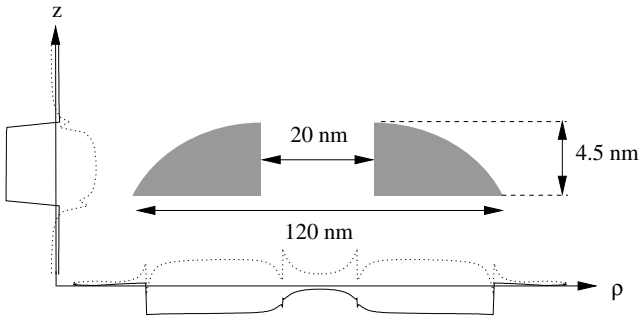

Figure 1. Cross-section of the investigated quantum ring and strain profile of $\varepsilon_{\parallel}$ (solid lines) and ε_{zz} (dotted lines). The radial strain profile is taken at half ring height and the vertical one at half section width. The confinement potential is $V_c = 0$ eV inside the ring (grey region) and $V_c = 0.77$ eV outside.

2. Theory

The one-band effective mass Hamiltonian for the electron states, including a magnetic field perpendicular to the ring plane, can be written in cylindrical coordinates and atomic units as

$$\mathcal{H}_e = \left(-\frac{1}{2}\nabla\left(\frac{1}{m^*(E_{n,m};\rho,z)}\nabla\right) + \frac{(B\rho)^2}{8m^*(E_{n,m};\rho,z)} + \frac{Bm}{2m^*(E_{n,m};\rho,z)} + \frac{1}{2}\mu_B g(E_{n,m};\rho,z)B\sigma + V_c(\rho,z) + a_c\varepsilon_{hyd}(\rho,z)\right), \quad (1)$$

where $m = 0, \pm1, \pm2, \ldots$ is the quantum number of the projection of the angular momentum onto the magnetic field (B) axis, n is the main quantum number, $V_c(\rho, z)$ is the finite confinement potential corresponding to the geometry shown in figure 1, and $m^*(E_{n,m};\rho,z)$ and $g(E_{n,m};\rho,z)$ stand for the energy- and position-dependent mass and Landé factor, respectively [17]. a_c denotes the hydrostatic deformation potential for the conduction band, and ε_{hyd} is the hydrostatic strain, which we calculate within the framework of the isotropic elastic theory [18, 19]. It should be noted that this theory allows for good strain estimates while preserving axial symmetry [20]. The strain profile along the radial direction at half ring height and that along the vertical direction at half ring cross-section are displayed in figure 1. Solid lines are used for lateral strain, $\varepsilon_{\parallel} = \frac{1}{2}(\varepsilon_{xx} + \varepsilon_{yy})$, and dotted lines are used for ε_{zz}. The main effect of hydrostatic strain is to increase the energy gap. This effect, along with the non-parabolicity of the conduction band, leads to increased electron effective masses for InAs. It is then possible to retrieve appropriate values of the mass to reproduce experimental results without having to invoke GaAs diffusion into the ring [15, 16]. Equation (1) is solved numerically using the finite-difference method on a two-dimensional grid (ρ, z). Ben Daniel–Duke boundary conditions are imposed [21].

The two-electron Hamiltonian can be written as

$$\mathcal{H}_{2e}(1,2) = \mathcal{H}_e(1) + \mathcal{H}_e(2) + V_{ee}(1,2), \quad (2)$$

where H_e is the single-particle Hamiltonian (equation (1)) and V_{ee} is the electron–electron Coulomb repulsion term. Equation (2) is solved by means of the configuration interaction method on the basis of the one-electron wavefunctions,

$$\psi_{n,m,\sigma} = f_{n,m}(\rho,z)\,e^{im\phi}|S\sigma\rangle, \quad (3)$$

where $f_{n,m}(\rho, z)$ is the eigenvector of equation (1) and $|S\sigma\rangle = |S\rangle|\sigma\rangle$ is the Bloch function for electrons, with the spin $\sigma = \uparrow$ or $\downarrow$. The matrix element of the electron–electron interaction

can be expressed as a five-dimensional integral,

$$\left\langle ij\left|\frac{1}{\epsilon^* r_{12}}\right|kl\right\rangle = \frac{1}{2\pi\epsilon^*}\int\int\int\int\int \mathrm{d}\rho_1\,\mathrm{d}\rho_2\,\mathrm{d}z_1\,\mathrm{d}z_2\,\mathrm{d}\Omega\cos(n\Omega)\,f_i(\rho_1,z_1)\,f_j(\rho_2,z_2) \times f_k(\rho_1,z_1)\,f_l(\rho_2,z_2)\frac{\rho_1\rho_2}{\sqrt{\rho_1^2+\rho_2^2+(z_2-z_1)^2-2\rho_1\rho_2\cos\Omega}}, \tag{4}$$

where ϵ^* is the effective dielectric constant, $n = (m_k - m_i)$ and $\Omega = \phi_2 - \phi_1$. Equation (4) is integrated using Monte Carlo routines. The two-electron wavefunction

$$\Psi_{M,S,N}(1,2) = \sum_{i,j} c_{i,j}^{M,S,N}\frac{1}{\sqrt{2}}(\psi_i(1)\psi_j(2) - \psi_i(2)\psi_j(1)), \tag{5}$$

is labelled by its total angular momentum z-projection $M = m_1 + m_2$, total spin $S = \sigma_1 + \sigma_2$ and main quantum number N.

The optical absorption intensities for intraband transitions between two-electron states are calculated within the electronic dipole approximation [22]. We assume non-polarized light, although most of the intensity arises from the in-plane light components. We also assume $T = 0$ K so that only transitions from the ground state are calculated. The transition probabilities are represented employing Lorentzian curves of half-width $\Gamma = 0.5$ meV, in order to obtain smooth spectra[3]. Hence the absorption coefficient can be written as

$$\alpha(E) = C\sum_{\mathrm{f}}\frac{E_{\mathrm{f}} - E_0}{1 + 4\left(\frac{E-(E_{\mathrm{f}}-E_0)}{\Gamma}\right)^2}|\langle\Psi_{\mathrm{f}}|\vec{\mu}|\Psi_0\rangle|^2. \tag{6}$$

Here C is a constant factor (which we arbitrarily set to one as we look for relative intensities). Ψ_{f} and Ψ_0 are the final and ground states, respectively. Their corresponding energies are E_{f} and E_0. The x-component of the two-particle dipole matrix element is defined by

$$\langle\Psi_{\mathrm{f}}|\mu_x|\Psi_0\rangle = -\langle\Psi_{\mathrm{f}}|(x_1+x_2)|\Psi_0\rangle \tag{7}$$

$$= -\sum_{i,j>i}\sum_{k,l>k} c_{i,j}^{f}c_{k,l}^{0}\left[\delta_{j,l}x_{ik} + \delta_{i,k}x_{jl} - \delta_{j,k}x_{il} - \delta_{i,l}x_{jk}\right], \tag{8}$$

where

$$x_{ik} = \int\int\int f_{n_i,m_i}(\rho,z)\mathrm{e}^{-\mathrm{i}m_i\phi}\rho\cos\phi f_{n_k,m_k}(\rho,z)\,\mathrm{e}^{\mathrm{i}m_k\phi}\rho\,\mathrm{d}\rho\,\mathrm{d}z\,\mathrm{d}\phi$$

$$= \tfrac{1}{2}(\delta_{m_i,m_k+1} + \delta_{m_i,m_k-1})\int\int f_{n_i,m_i}(\rho,z)\,f_{n_k,m_k}(\rho,z)\rho^2\,\mathrm{d}\rho\,\mathrm{d}z. \tag{9}$$

The y- and z-components of the transition moment are analogously defined.

3. Results and discussion

We investigate a self-assembled InAs ring embedded in a GaAs matrix. Lacking precise knowledge on the composition, size and shape of self-assembled structures, our main goal is to qualitatively study the role of electron–electron interactions. Making arbitrary assumptions about the effects of diffusion and segregation would allow for a better fit of the experimental results at the expense of introducing subjectivity. Thus, we simply use the shape and dimensions of a typical InAs ring observed by atomic force micrography [5, 23] and assume a pure InAs

[3] The value $\Gamma = 0.5$ meV is just an empirical parameter to simulate a smooth spectrum.

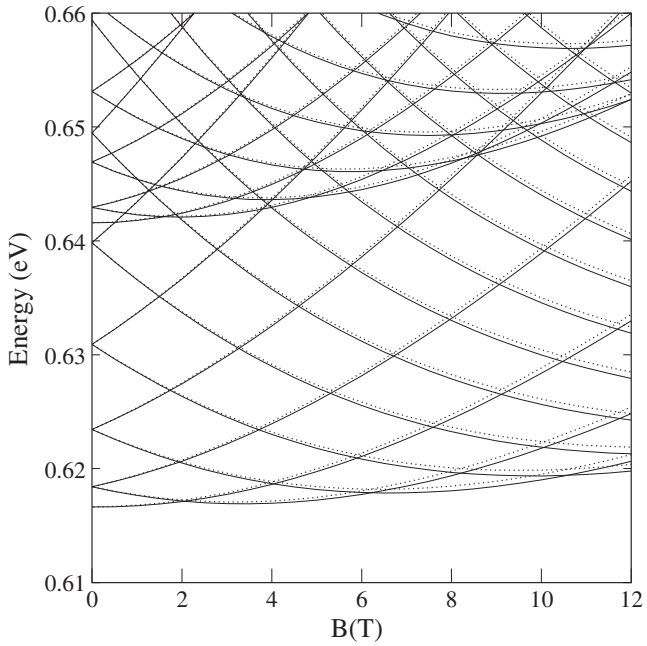

Figure 2. Low-lying energy levels of a single electron in the quantum ring versus magnetic field. Solid curves are used for the spin $\sigma = \uparrow$ states and dotted curves for the spin $\sigma = \downarrow$ states.

composition[4]. For similar reasons, we neglect the presence of a wetting layer. The shape of our ring is a cut torus (see cross-section in figure 1). The inner radius is 10 nm and the outer radius 60 nm [5]. Following recent measurements [23], 4.5 nm height is set at the inner edge of the ring cross-section and then we let it decrease as a spherical casket. We use an electron band-edge effective mass for InAs(GaAs) $m^* = 0.028(0.067)$, energy gap $E_g = 0.42(1.52)$ eV, split-off $\Delta = 0.38(0.34)$ eV and hydrostatic deformation potential $a_c = -6.66(-9.3)$ eV [20, 24]. The corresponding conduction band offset is 0.77 eV, and the effective dielectric constant is 12.4. The configurations interaction calculations include all the single-particle states up to 35 meV away from the ground state. We have checked that by enlarging this basis set no significant changes in the low-lying two-electron states are achieved within the range of the magnetic field that is being studied (0–12 T).

Figure 2 illustrates the low-lying single-electron energy levels versus magnetic field. Solid curves represent $\sigma = \uparrow$ states, and dotted curves $\sigma = \downarrow$ states. Two sets of lines corresponding to the ground $n = 1$ and first excited $n = 2$ states can be seen. The first set ($n = 1, |m| = 0, 1, 2\ldots$) begins at about 617 meV and the second one ($n = 2, |m| = 0, 1, 2\ldots$) at about 641 meV. In the presence of a magnetic field, the energy of the ground state describes aperiodic oscillations as expected from the AB effect in quantum rings with finite width [17]. Figure 2 is similar to the electron energy spectrum in [16]. The most significant differences shown in figure 2 are the magnitude of the binding energies (about 600 versus 200 meV in [16]) and the energy spacing between levels with $\Delta m = \pm 1$ at zero magnetic field (about twice as much as in [16]). The first difference comes from the hydrostatic strain. The second is due to the

[4] Recent evidence about the synthesis of InP/GaAs self-assembled rings indicates that the shape transformation from dots to rings is not accompanied by compositional changes [2]. Besides, an InGaAs alloy would yield similar results to those we predict here because the increased electron effective mass due to the presence of Ga is compensated by the weaker strain effects which, as mentioned in section 2, also lead to increased effective masses.

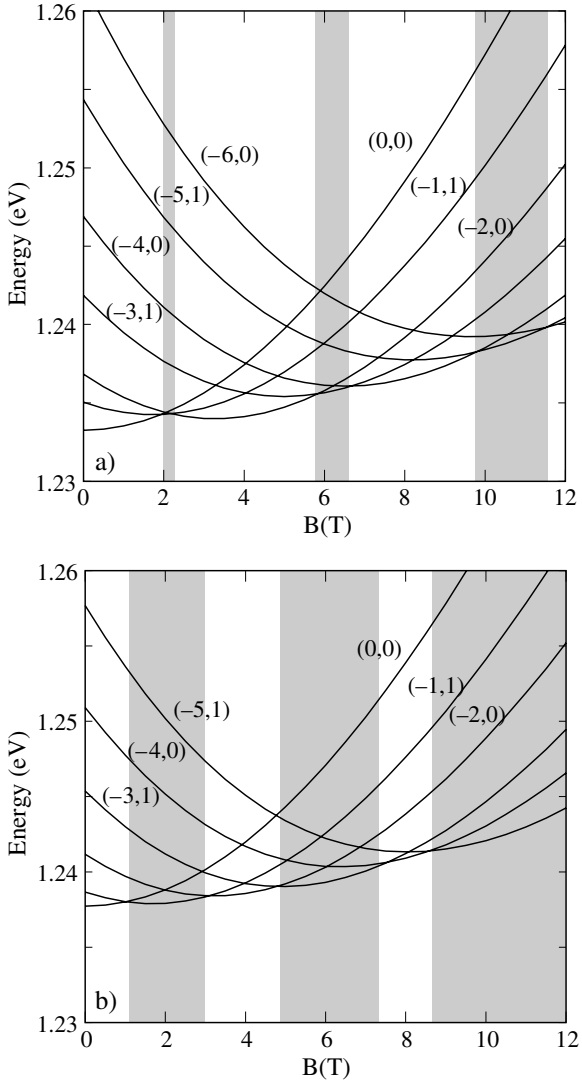

Figure 3. Two-electron energy levels versus magnetic field in the absence (a) and presence (b) of electron–electron Coulomb interaction. Only levels that become the ground state in a given magnetic field window are shown. Grey-shaded regions indicate windows where the ground state has a total spin of $S = 1$.

current ring cross-section shape which allows the charge density maximum to be located at values of ρ below those found in [16], yielding, then, larger contributions of the centrifugal term in the Hamiltonian (1). It should also be noted that the energy spacing between levels with $\Delta n = 1$ in figure 2 is similar to that found within a similar three-dimensional single-particle model [17].

Figure 3 shows the two-electron ground state versus magnetic field without (a) and with (b) Coulomb interaction. The states are labelled according to their total angular momentum z-projection and total spin (M, S). Grey-shaded regions represent magnetic field windows where the ground state has spin one (triplet). At $B = 0$ the ground state is $(0, 0)$ in both cases

(with and without Coulomb interaction). As the magnetic field increases, states with lower M become more stabilized, eventually replacing the $(M+1)$ ones as the ground state. As a result, the ground state shows a succession of decreasing M and spin oscillation (singlet–triplet–singlet–triplet$\cdots$) that characterizes the interplay between the Zeeman term and the ringlike confinement [7]. When no Coulomb interaction is included, the ground state is predominantly singlet ($S = 0$), although the contribution of the atomic Zeeman term in the single-particle Hamiltonian (equation (1)) gives rise to windows of the magnetic field where $S = 1$ levels become the ground state (grey-shaded regions). Such windows, which are relatively wide even at moderate magnetic fields, are not found when the atomic Zeeman term is neglected [7, 10, 11]. Therefore, figure 3(a) shows that the contribution of the atomic Zeeman term, even though small in magnitude, can strongly modify the energy structure of electrons in a self-assembled ring. When the Coulomb interaction is considered (figure 3(b)), all the states are shifted upwards due to electron–electron repulsion. The lowest-lying levels experience a stronger Coulomb interaction and so at $B = 0$ the ground state $(0, 0)$ is closer to the first excited state $(-1, 1)$ than in the non-interacting case. Moreover, the $S = 1$ triplet states are stabilized by the exchange interaction and they come down in energy with respect to the singlets. As a result, the values of the magnetic field corresponding to the first crossings of the ground state are approximately halved as compared to those of the non-interacting picture. This is known as the 'fractional AB effect' [10]. This effect is strongly dependent on the size of the quantum ring. Figure 3(b) gives an estimation for an InAs self-assembled ring with the dimensions observed in atomic force micrographs. In our calculations, the halving of the spin singlet domains is approximate only at low values of the magnetic field. At high values, the spin singlet domains are almost suppressed and the ground state has predominantly spin one (triplet). This is due to the enhancement of electron–electron interactions and atomic Zeeman splitting with increasing magnetic field. The first crossings in figures 3(a) and (b) take place at similar magnetic field values to those predicted by Puente and Serra for both interacting and non-interacting electrons [8], although for the increasing field we find a larger number of crossings.[5]

It is worthwhile pointing out that the net Coulomb interactions we find at $B = 0$ are in the 3–5 meV range. They are smaller than the ones predicted by the two-dimensional models (between 7 and 11 meV) [7, 9] because two-dimensional models overestimate Coulomb interactions due to the infinite confinement in the vertical direction. Our Coulomb interaction energies are also below the 20 meV inferred by Lorke *et al* using capacitance spectroscopy [5]. We have determined that such a large Coulomb energy cannot be achieved with our model even for narrow-width rings holding a 10 nm inner radius, because the charge density spreads over the inner core of the ring before reaching such a strong interaction. Therefore, our calculations suggest that the missing central part of the ring cannot be responsible for any surprisingly large Coulomb interaction as pointed out in [5].

In figure 4 we plot the FIR absorption of the two-electron ring without (a) and with (b) Coulomb interaction for $B = 0, 0.5, 1, 1.5, \ldots, 12$ T. The intensities are displayed in arbitrary units and they are offset for the sake of clarity. In the non-interacting picture two sets of resonances can be easily distinguished, a low-lying $\Delta N = 0$ one and a high-lying $\Delta N = 1$ one. At zero magnetic field, the low-lying resonance consists of a single peak at 1.8 meV and the high-lying one is also a single peak at 26.3 meV. When the magnetic field is switched on, both the low-lying and high-lying resonances exhibit Zeeman splitting. The single peaks at $B = 0$ now split into two smaller branches, one at slightly lower energies related to $\Delta M = -1$ transitions and the other at slightly higher energies related to $\Delta M = 1$ transitions.

[5] See [16] for a physical interpretation of the larger number of crossings in our calculations.

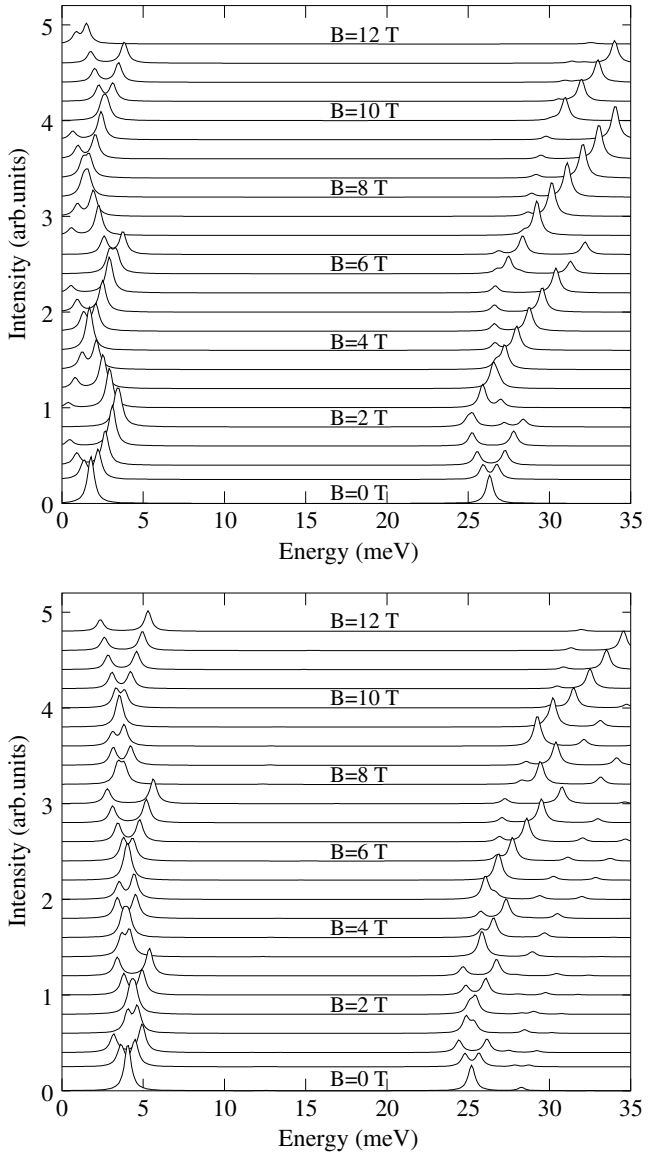

Figure 4. Two-electron FIR absorption in the absence (a) and presence (b) of electron–electron Coulomb interaction at $T = 0$ K. The spectra are calculated for magnetic fields $B = 0$–12 T in steps of 0.5 T. The intensities are in arbitrary units and the curves have been offset for clarity.

In general the $\Delta M = 1$ branch is more intense than the $\Delta M = -1$ one. As the magnetic field increases, the energy of the low-lying $\Delta M = 1$ resonances progresses in a zigzag manner, while the high-lying $\Delta M = 1$ branch experiences sudden bumps. This behaviour is originated by the AB oscillations of the ground state energy (see figure 3(a)). The absorption spectrum of interacting particles roughly resembles that without Coulomb interaction. However, some important differences can be underlined. First, the peaks at zero magnetic field get closer. Thus, the low-lying peak is now at 4.1 meV and the high-lying one is at 25.2 meV. In addition, a new smaller peak arises at 28.3 meV. This peak originates from the mixing of different

angular momenta and spins induced by the Coulomb interaction. Second, the intensity of the resonances is quite different. This can be seen for example in the relative intensities of the low-lying $\Delta M = 1$ and $\Delta M = -1$ branches, which are now of a similar size for all magnetic fields. Third, the symmetry changes of the ground state occur at different values of the field due to the fractional AB effect (see figure 3(b)) and this has a profound impact on the possible transitions at each value of B.

Figure 4 is very different from the absorption spectrum of a self-assembled ring which is obtained with the usually employed parabolic confinement potential [6, 7]. Nonetheless, it strongly resembles the calculated magneto-absorption spectrum of the quantum ring $V3$ in [8]. Therefore, our model also suggests that a single quantum ring cannot account for all the experimental FIR resonances and at least a second type of ring must be present in the sample measured by Lorke *et al* [5]. This second type of ring must be responsible for the resonances between 10 and 20 meV. The agreements of the two calculated absorption spectra (interacting and non-interacting) with the high-energy experimental resonances (marked with dots in figure 2(b) of [5]) are rather similar[6]. Therefore, our model indicates that Lorke's experiment can be roughly described within the single-particle approximation, although higher-resolution experiments should find clear manifestations of electron–electron interaction effects.

4. Conclusion

In conclusion, we have studied the electron energy structure and FIR absorption of one and two electrons in a self-assembled InAs/GaAs quantum ring in a magnetic field. The atomic Zeeman effect and electron–electron interactions have been found to induce significant changes in the energy structure and FIR absorption. The Coulomb exchange interaction yields visibly aperiodic fractional AB oscillations of the ground state energy as well as a rapid narrowing of the magnetic field windows corresponding to spin zero (singlet) ground state. Our 3D model calculations compares well with FIR resonance energies and oscillator strengths obtained in [8] with a modified form of the parabolic potential for the inner radius of the ring. Here the results are achieved without any parameter fitting, therefore giving strong support to their interpretation of [5] experiments on self-assembled ring spectroscopy. These results also suggest that the parabolic form of the confinement potential used for mesoscopic rings [12] is unsuitable for self-assembled rings, as it poorly describes the effect of the inner radius.

Acknowledgments

We wish to thank A Lorke for helpful discussion. Financial support from an MEC-FPU grant, MEC-DGI project CTQ2004-02315/BQU and UJI-Bancaixa project P1-B2002-01 is gratefully acknowledged.

References

[1] Garcia J M, Medeiros-Ribeiro G, Schmidt K, Ngo T, Feng J L, Lorke A, Kotthaus J and Petroff P M 1997 *Appl. Phys. Lett.* **71** 2014
[2] Raz T, Ritter D and Bahir G 2003 *Appl. Phys. Lett.* **82** 1706
[3] Aharonov Y and Bohm D 1959 *Phys. Rev.* **115** 485

[6] This agreement is only moderate. It can be significantly improved by assuming slightly different dimensions to those used in this study [25]. However, as mentioned before, the goal of this work is the qualitative study of electron–electron interactions. Therefore, we only present here the results obtained using the average dimensions of uncapped InAs self-assembled rings.

[4] Wendler L, Fomin V M, Chaplik A V and Govorov A O 1996 *Phys. Rev.* B **54** 4794
[5] Lorke A, Luyken R J, Govorov A O, Kotthaus J P, Garcia J M and Petroff P M 2000 *Phys. Rev. Lett.* **84** 2223
[6] Emperador A, Pi M, Barranco M and Lorke A 2000 *Phys. Rev.* B **62** 4573
[7] Hu H, Zhu J L and Xiong J J 2000 *Phys. Rev.* B **62** 16777
[8] Puente A and Serra L 2001 *Phys. Rev.* B **63** 125334
[9] Xia J B and Li S S 2002 *Phys. Rev.* B **66** 035311
[10] Niemelä K, Pietiläinen P, Hyvönen P and Chakraborty T 1996 *Europhys. Lett.* **36** 533
[11] Emperador A, Pederiva F and Lipparini E 2003 *Phys. Rev.* B **68** 115312
[12] Chakraborty T and Pietiläinen P 1994 *Phys. Rev.* B **50** 8460
[13] Peeters F M and Schweigert V A 1996 *Phys. Rev.* B **53** 1468
[14] Li S S and Xia J B 2001 *J. Appl. Phys.* **89** 3434
[15] Climente J I, Planelles J and Jaskolski W 2003 *Phys. Rev.* B **68** 075307
[16] Planelles J, Jaskolski W and Aliaga J I 2002 *Phys. Rev.* B **65** 033306
[17] Voskoboynikov O, Li Y, Lu H M, Shih C F and Lee C P 2002 *Phys. Rev.* B **66** 155306
[18] Downes J R, Faux D A and O'Reilly E P 1997 *J. Appl. Phys.* **81** 6700
[19] Davies J H 1998 *J. Appl. Phys.* **84** 1358
[20] Tadić M, Peeters F M, Janssens K L, Korkusiński M and Hawrylak P 2002 *J. Appl. Phys.* **92** 5819
[21] Harrison P 2000 *Quantum Wells, Wires and Dots* (Guilford: Wiley)
[22] Loehr J P 1998 *Physics of Strained Quantum Well Lasers* (Boston: Kluwer–Academic)
[23] Barker J A, Warburton R J and O'Reilly E P 2004 *Phys. Rev.* B **69** 035327 The cross-section of an InAs self-assembled ring, taken with an atomic force microscope, can be seen in figure 4 of this work
[24] Vurgaftman I, Meyer J R and Ram-Mohan L R 2001 *J. Appl. Phys.* **89** 5815
[25] Planelles J and Climente J I 2004 *Preprint* cond-mat/0412552